

## Structural and Magnetotransport Properties of $\text{YbRh}_2\text{Si}_2$ and its Co- and Ir-Substituted Derivatives $\text{Yb}(\text{Rh}_{1-y}\text{Ir}_y)_2\text{Si}_2$ and $\text{Yb}(\text{Rh}_{1-x}\text{Co}_x)_2\text{Si}_2$

Steffen Wirth, Horst Borrmann, Manuel Brando, Ulrich Burkhardt, Raul Cardoso-Gil, Stefan Ernst, Sven Friedemann<sup>1</sup>, Philipp Gegenwart<sup>2</sup>, Christoph Geibel, Stefan Kirchner<sup>3</sup>, Cornelius Krellner, Niels Oeschler, Silke Paschen<sup>4</sup>, Qimiao Si<sup>5</sup>, Tanja Westerkamp, Gertrud Zwicky<sup>6</sup>, Yuri Grin, and Frank Steglich

Phase transitions are ubiquitous in nature. In the cases that are encountered in daily life (like the melting of ice to water) temperature is the parameter that drives these phase transitions. Recently however, there is growing interest of the condensed matter physics community in such phase transitions which are not thermally induced. A phase transition at absolute zero temperature ( $T = 0$ ) driven by a non-thermal control parameter is termed a quantum phase transition. If this phase transition is continuous it is a so-called quantum critical point (QCP) which results solely from quantum fluctuations because the thermal fluctuations are cut off for  $T \rightarrow 0$ .

Heavy fermion metals which typically contain  $4f$  or  $5f$  elements (*e.g.* Ce, Yb or U) are so far the only systems in which signatures of such QCPs have unambiguously been identified [1,2]. In these materials, the ground state sensitively depends on the balance between two competing interactions, which are both determined by the hybridization strength  $J$  between the spins of the localized  $4f$  or  $5f$  shells and those of the conduction electrons [3]. On the one hand, the Kondo entanglement results in a screening of these local spins resp. the associated local moments below a Kondo temperature  $T_K$ , giving rise to a paramagnetic ground state. On the other hand, the indirect exchange coupling, the so-called RKKY interaction, can mediate long-range magnetic ordering. As the involved energy scales are small, varying an external control parameter like pressure, chemical composition or magnetic field may influence the hybridization  $J$  such that the system's ground state can be tuned between the magnetically ordered one and the paramagnetic Fermi liquid phase resulting in the above-mentioned QCP.

The heavy fermion metal  $\text{YbRh}_2\text{Si}_2$  has recently turned out to be an ideal model system for the study of the Kondo effect and quantum criticality for several reasons: i)  $\text{YbRh}_2\text{Si}_2$  is one of the heaviest heavy fermion metals. Upon cooling below the

single-ion Kondo temperature  $T_K \approx 80$  K, a strong increase of the effective charge-carrier mass is observed. The latter can reach up to several hundred times the bare electron mass [4] as evidenced by a Sommerfeld coefficient  $\gamma > 1 \text{ Jmol}^{-1}\text{K}^{-2}$  at  $T < 0.1$  K. ii) In contrast to many other heavy fermion systems,  $\text{YbRh}_2\text{Si}_2$  does not show any sign of superconductivity down to 6 mK, consequently allowing for detailed low-temperature electronic studies. iii) In  $\text{YbRh}_2\text{Si}_2$ , the Néel temperature  $T_N = 70$  mK is small, *i.e.*, the energy scales given by  $T_N$  and  $T_K$  are well separated. Further,  $T_N$  can be suppressed by applying a small magnetic field ( $\approx 60$  mT within the magnetically easy  $ab$  plane) at which the QCP is accessed [5]. The QCP in  $\text{YbRh}_2\text{Si}_2$  is discussed [6] to follow the rather unconventional Kondo-breakdown scenario, *i.e.* the heavy quasiparticles disintegrate [7] at around an additional energy scale  $T^*(B)$ . iv) Single crystals of excellent quality are available, with the latest generation of crystals exhibiting [8] residual resistivities of  $\rho_0 \approx 0.5 \mu\Omega\text{cm}$ .

In this report we demonstrate by Scanning Tunneling Spectroscopy (STS) that the heavy quasiparticles are well defined below  $T_K$ , and develop spatial coherence below a characteristic temperature  $T_L \approx 30$  K [9]. For even lower temperatures approaching  $T^*(B)$  we present new results of in-depth Hall measurements providing further support for the above-mentioned Kondo-breakdown scenario and an energy-over-temperature scaling. Our findings are corroborated by renormalized bandstructure calculations [10].

$\text{YbRh}_2\text{Si}_2$  crystallizes in a tetragonal  $\text{ThCr}_2\text{Si}_2$  structure [11] (Fig. 1 top). In an effort to probe a possible correlation of the lattice parameters with the residual resistance ratio (RRR), samples of very different RRR were investigated by high-precision XRD and WDXS measurements. The lattice parameters were obtained from powdered single crystals and polycrystalline specimens by fitting the  $2\theta$  values of 20 reflections within a range

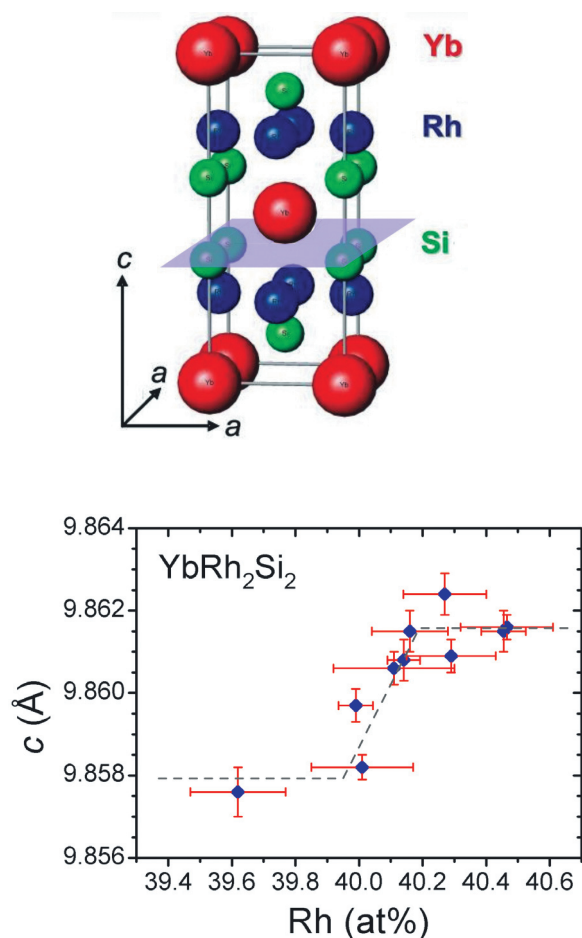


Fig. 1 top: Tetragonal crystal structure of  $\text{YbRh}_2\text{Si}_2$ . The magenta plane indicates the cleaving plane. Bottom: Lattice parameter  $c$  in dependence on the Rh content. A narrow homogeneity range from 40.0 at.% – 40.2 at.% Rh is inferred.

$15^\circ \leq 2\theta \leq 95^\circ$ . While the lattice parameter  $a$  remains unchanged within the estimated standard deviation (e.s.d.) for all samples investigated, the lattice parameter  $c$  shows a non-monotonic dependence on the Rh content (Fig. 1, bottom). For Rh contents below 40.0 at.% and above 40.2 at.%, the value of  $c$  stays unchanged within one e.s.d. In the intermediate range of Rh concentration an increase of  $c$  from 9.858(1) Å to 9.8615(10) Å with increasing Rh content is observed. Although the measured values of the lattice parameters and Rh concentrations are at the experimental limits, the existence of a very narrow homogeneity range – most probably  $\text{YbRh}_{2+z}\text{Si}_{2-z}$  – may be established from these data. This finding emphasizes the sensitivity of the transport properties with respect to the sample quality in  $\text{YbRh}_2\text{Si}_2$  which is at the resolution limits of XRD characterization.

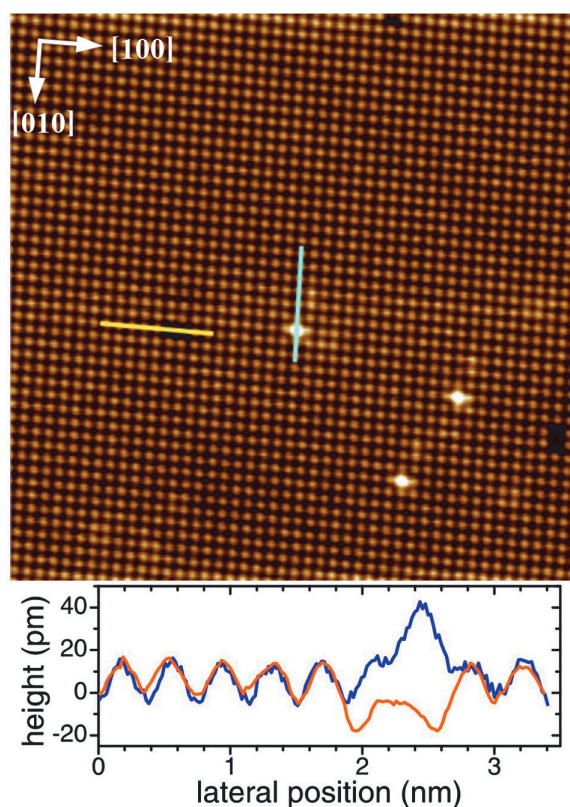


Fig. 2: Topography on a single crystalline  $\text{YbRh}_2\text{Si}_2$  sample cleaved *in situ* and at low temperature ( $\sim 20$  K) along the crystallographic  $ab$  plane. Shown area: 18 nm  $\times$  18 nm obtained at  $T = 4.6$  K. The distance between the surface atoms amounts to 4.0 Å, in nice agreement with the lattice parameter  $a = 4.007$  Å. The line scans in the lower part (taken along the two lines of similar color in the topography) visualize the excellent atomic resolution as well as the nature of the two types of defects encountered.

For our STM investigations high quality single crystals of  $\text{RRR} \geq 20$  were used. The orientation of the single crystals was obvious from their shape as the  $ab$  plane formed smooth and extended surfaces of the platelet-like single crystals. So far, six single crystals were cleaved *in situ* at low temperatures ( $\sim 20$  K) along the  $ab$  plane, *i.e.* perpendicular to the [001] direction. The topography (Fig. 2) obtained at 4.6 K evidences an excellent cleave. A Fast Fourier Transformation (FFT) of the surface pattern reveals a perfect fourfold symmetry of the surface atoms with distances of 4.0 Å, in excellent agreement with the lattice parameter  $a = 4.007$  Å. Taking into account the earlier observation of a cleavage between the Yb and Si bonds [12], we propose that Figure 1 represents a Si terminated surface. An extremely low defect density is found for all our samples, in concert with the high RRR.

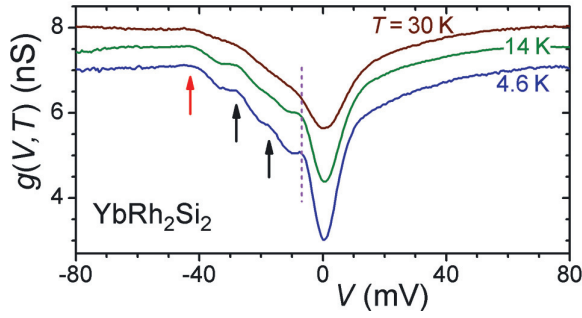


Fig. 3: Differential conductance  $g(V, T)$  as measured by STS on  $\text{YbRh}_2\text{Si}_2$ . Beside the dominating dip in  $g(V, T)$  at around zero bias, several features can be identified. The peaks marked by arrows correspond to CEF excitations whereas the more strongly temperature dependent peak at  $\approx 6$  mV is associated with the formation of the Kondo lattice.

The most common defects in the structure of  $\text{YbRh}_2\text{Si}_2$  should be an occupation of Si-sites by Rh, occupation of Rh sites by Si and Si voids. The line scans through the two observed types of defects clearly indicate that these defects cannot be caused by missing or additional atoms. Rather, the most numerous defects observed – the single protrusions – could originate from a larger Rh ion occupying a Si site at the surface (blue line in Fig. 2). This again indicates that the surface shown in Figure 2 is Si terminated. This assignment can also explain the dumbbell-shaped dents (yellow line in Fig. 2): If a smaller Si occupies a Rh site within the second-to-topmost layer the two adjacent Si in the topmost layer should be affected. Here we note that the defect structure as exemplified in Figure 2 has been observed over very large areas and on different samples. Only in one case did we observe a surface of different type (likely Yb-terminated) characterized by individual dents of about 40 pm height change. It should be emphasized that specifically the line scan perpendicular to the fast scan direction of the STM topography (blue line) underlines the quality of our data with a noise level of about 2 pm.

Differential conductances  $g(V, T) = dI/dV|_T$  obtained by STS on such excellent surfaces at different temperatures are exemplified in Figure 3. These spectra are dominated by a gap-like feature around zero bias. At low temperatures, additional peaks can be recognized which can be distinguished by their temperature dependences as discussed below. An analysis of the position in energy of the three peaks marked by the arrows in Figure 3 yields  $-17$  meV,  $-27$  meV and  $-43$  meV. These energies are in

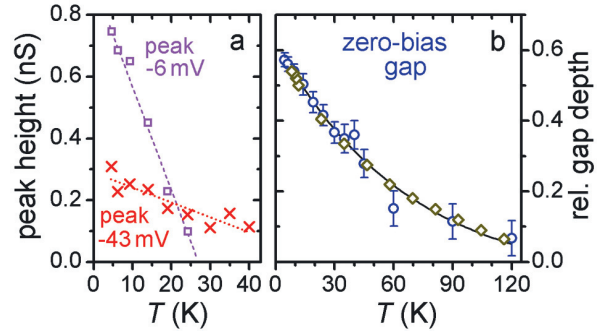


Fig. 4: Temperature evolution of the different features observed in STS. a) Peak height of the CEF excitations exemplified by the most prominent peak at  $-43$  mV in comparison to the height of the peak at  $-6$  mV related to the Kondo lattice formation. b) Relative depth of the zero-bias gap (“Kondo dip”) from experiment (blue circles) and NCA calculations (diamonds). The line represents theoretically predicted logarithmic decay.

excellent agreement with those of the crystalline electric field (CEF) excitations as observed by inelastic neutron scattering (INS) [13]. This first (to the best of our knowledge) observation of CEF excitations by STS is of utmost importance as, on the one hand, it indicates that we truly measure bulk properties of our  $\text{YbRh}_2\text{Si}_2$  samples and, on the other hand, it supports our conjecture of a Si terminated surface [9]. Finding these peaks so close to the Fermi level  $E_F$  points at the Kondo effect to be at play and shifting the spectral weight. The temperature dependence of the most prominent peak at  $-43$  mV is presented in Figure 4a.

The hybridization of conduction and  $4f$  electrons, *i.e.* the local Kondo entanglement, modifies the local density of states  $\rho$  (DOS) which determines the measured  $g(V, T)$ . In general,  $\rho(E)$  is to be calculated from the Green function

$$\varrho(E) = -\frac{1}{\pi\hbar} \text{Im} \left( \text{Tr}_{\mathbf{r}} \mathcal{G}_0^+(\mathbf{r}, \mathbf{r}', E) \right). \quad (1)$$

We followed two different approaches to evaluate eq. (1) relying on i) the non-crossing approximation (NCA) [14] generalized to the multi-orbital case with finite Coulomb repulsion or ii) a renormalized band structure calculation [10].

In the heavy fermion metals tunneling into two channels, so called co-tunneling, is possible: into the conduction band as well as into the heavy quasiparticle bands [15,16]. Relying on the observation of a Si terminated surface only tunneling into the conduction band is considered [9]. Note that

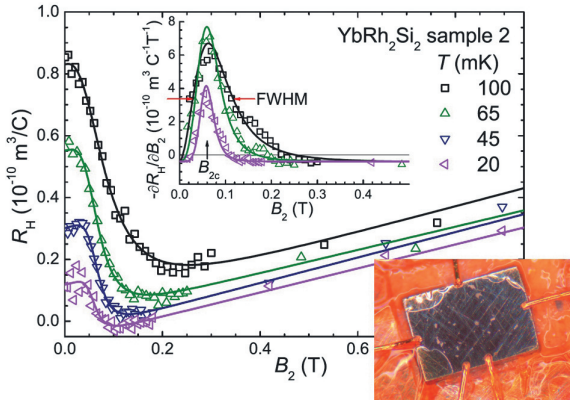


Fig. 5: Hall coefficient  $R_H$  as function of field  $B_2$  at selected temperatures measured in the crossed-field setup. The inset shows the derivative of  $R_H(B_2)$  from which the FWHM was determined. The derivative allows for a clear distinction between the critical and background component. The lines are fit results; for details see [19]. Also shown is a photograph of a  $\text{YbRh}_2\text{Si}_2$  single crystal contacted for magnetotransport measurements (sample size is approximately  $0.8 \text{ mm} \times 0.6 \text{ mm}$ , thickness  $\sim 80 \mu\text{m}$ ).

such an approximation still covers the essence of the Kondo effect due to the afore-mentioned hybridization. In fact, it is this Kondo entanglement that results in a reduced  $g(V, T)$  around zero bias as part of the conduction electrons probed by tunneling are “bound” within the quasiparticles. The zero-bias gap in  $g(V, T)$  is nicely reproduced by the NCA calculations. The relative gap depth (defined as the difference of actual  $g(V=0, T)$  and the “un-gapped” conductance value extrapolated from those at  $|V| > 80 \text{ mV}$ , normalized to the latter) obtained by STS and by NCA calculations agree very well in their temperature dependences, Figure 4b and follow a logarithmic decay at temperatures in the order of  $T_K$  [17].

We now turn to the peak at  $-6 \text{ meV}$ . The temperature dependence of its height is included in Figure 4a. It decays much faster than the CEF peak and disappears at  $T_L \approx 27 \text{ K}$ . An analysis of the peak width also yields  $T_L = (30 \pm 6) \text{ K}$ . This temperature coincides with the Kondo temperature ( $29 \text{ K}$ ) of the *lowest-lying* CEF Kramers doublet as determined from resistivity [11,18] and thermopower [18] measurements. Moreover, our renormalized band structure calculations did not provide any other indication for its origin than the hybridization gap [10].

These results [9] allow for important insight into the thermal evolution of the Kondo effect in  $\text{YbRh}_2\text{Si}_2$ : The observed zero-bias gap develops below  $T_K = 80 \text{ K} - 100 \text{ K}$ , *i.e.*, a temperature scale set by the single ion Kondo temperature which, however, averages over all involved CEF levels [19]. Upon cooling below  $T_L \approx 30 \text{ K}$ , only the lowest-lying CEF Kramers doublet is occupied. This allows for the development of a spatially coherent state which is manifested by an additional peak in  $g(V, T)$  at  $-6 \text{ mV}$  reflecting a “Kondo lattice resonance” related to an incomplete hybridization gap.

In the following we study  $\text{YbRh}_2\text{Si}_2$  at even lower temperatures in an effort to scrutinize the Kondo-breakdown scenario discussed for this material. It is speculated that the quasiparticles disintegrate and, consequently, the Fermi-surface volume is expected to undergo a discontinuous change at the QCP. Based on this, measurements which probe the volume of the Fermi sea were suggested [20] as an experimental tool to discriminate between the local scenario discussed above and the more conventional quantum generalization of the Ginzburg-Landau-Wilson theory of finite-temperature phase transitions that assumes magnetic order to arise via a spin-density-wave of the heavy quasiparticles [21–23]. In view of the experimental conditions required (see below) we continued earlier Hall effect measurements [6] with improved precision and on single crystals of improved quality. Special attention was paid to careful temperature, field and alignment control in the so called crossed-field setup which allows to disentangle the Hall response and the tuning effect by applying orthogonal magnetic field. Results of the initial-slope (with respect to the field dependence of the Hall resistivity) Hall coefficient  $R_H$  in dependence of the tuning field  $B_2$  at several temperatures are presented in Figure 5. In these measurements [24], a critical component at small field (below  $0.2 \text{ T}$ ) can clearly be distinguished from a background linear increase at higher fields due to Zeeman splitting of the underlying band structure. For further analysis we consider its derivative  $-\partial R_H / \partial B_2$  (inset to Fig. 5) and specifically, the full width at half maximum (FWHM). It is this width that is required to be zero in the zero-temperature limit if a jump of the Fermi volume takes place (of course, there has to remain a finite jump height in  $R_H$  for  $T \rightarrow 0$ , *cf.* [25]). As indeed seen in Figure 6a, our measurements indicate that the  $\text{FWHM}(T)$  obtained for dif-

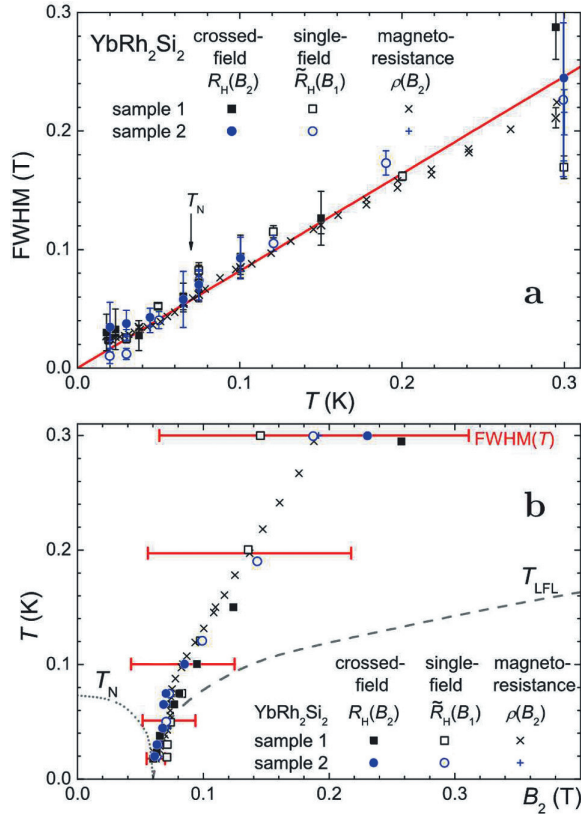


Fig. 6: a) FWHM of the crossover determined from Hall effect and magnetoresistance measurements. The solid line represents a linear fit to all data. Within the experimental accuracy this fit intersects the ordinate at the origin. b) Position of the Hall crossover in the temperature-field phase diagram. The red bars reflect the FWHM at selected temperatures, see a). Results of single-field and magnetoresistance measurements as well as the boundaries of the antiferromagnetic phase ( $T_N$ ) and the Fermi-liquid regime ( $T_{LFL}$ ) are shown for comparison.

ferent samples and quantities extrapolates to zero for  $T \rightarrow 0$ . In line with our renormalized band structure calculations, the “small” ( $4f$ -core) and “large” ( $4f$ -itinerant) Fermi surfaces at fields below and above the critical  $B_2$  in  $\text{YbRh}_2\text{Si}_2$  are respectively dominated by two hole and one hole/one electron Fermi-surface sheets [10]. Correspondingly, the step of  $R_H$  is expected to be negative once  $B_2$  increases through its critical value at the QCP, as is indeed seen here.

The resulting  $B$ - $T$  phase diagram is presented in Figure 6b. The markers indicate the position of the midpoint of the crossover obtained from the crossed-field experiment as well as from ordinary (single-field) Hall and longitudinal magnetoresistance measurements (for details of the analysis see [10]). The horizontal bars visualize the width of

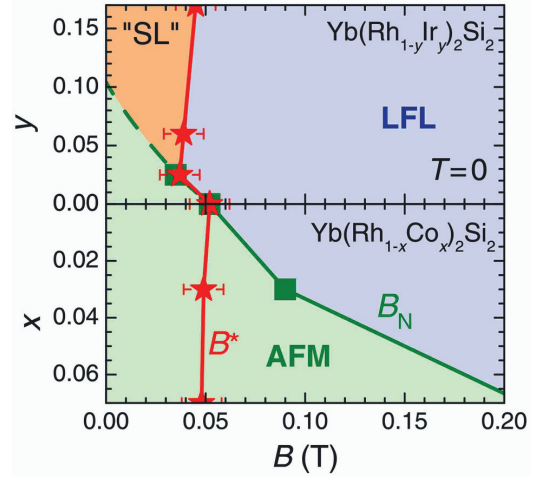


Fig. 7: Zero-temperature phase diagram based on [21]. The critical field  $B_N$  of the antiferromagnetically ordered phase (AFM) and the critical field of the  $B^*(T)$ -line are presented as a function of iridium (upper part) and cobalt substitution (lower part). The Fermi-liquid regime is indicated by LFL. Also shown is the region with in which a new phase, possibly a spin liquid (SL) phase is formed.

the crossover which rapidly increases with  $T$ . This phase diagram can favorably be compared to results of numerous other measurements [7], an agreement that corroborates our findings.

An intriguing observation is the linear dependence of the FWHM on temperature, Figure 6a, with essentially no sample dependence. This finding is compatible with a quantum-dynamical scaling of the critical single-electron excitations. A reconstruction of the Fermi surface across the QCP implies that the single-electron Green’s function contains a singularity at the QCP. Because the single-electron Green’s function characterizes each of the two Fermi liquids on either side of the QCP, this is related to the critical relaxation rate,  $\Gamma(\mathbf{k}_F, T)$ , of the single-electron states. While at  $T = 0$  the change from one Fermi surface to the other is sharp, the continuous crossover between the Fermi surfaces at finite temperature is controlled by the single-electron relaxation rate  $\Gamma(\mathbf{k}_F, T)$ . This is consistent with the  $E/T$  form in the dynamical critical scaling and points to the microscopic many-body excitations of a collapsing Fermi surface as the underlying mechanism of the macroscopic critical fluctuations.

Further insight into quantum criticality can be gained by substitution studies. Small isoelectronic substitutions on the Rh site in  $\text{YbRh}_2\text{Si}_2$  can be considered as chemical pressure [26,27]: smaller

Co induces a volume decrease and therefore, acts as positive pressure whereas bigger Ir corresponds to negative pressure due to a larger unit cell volume. Such a picture is confirmed by magnetization measurements on  $\text{YbRh}_2\text{Si}_2$  under hydrostatic pressure [28]. The volume effect shifts the magnetic transition temperature  $T_N$  and the critical field  $B_N$  (at which  $T_N \rightarrow 0$ ) as expected for Yb systems. By contrast, the position of the Kondo-breakdown energy scale  $T^*$  and its critical field  $B^*$  at which  $T^* \rightarrow 0$  is almost not altered. As a consequence, the coincidence of the Fermi-surface reconstruction and the antiferromagnetic instability (as observed in the stoichiometric compound) appears to be lifted for most of the substituted samples, Figure 7. This detachment specifically for Ir substitution  $y \geq 0.06$  raises the pressing question about the fate of the magnetic moments: On the one hand, they appear not to order and, on the other hand, they cannot be fully screened, as this only takes place at fields larger than  $B^*$ . Consequently, one may speculate that they form a new type of metallic spin-liquid phase hitherto not known in Kondo lattice systems. This could arise, for instance, from frustration between different magnetic interactions [29].

An intriguing part of the phase diagram is located close to the stoichiometric  $\text{YbRh}_2\text{Si}_2$ : Remarkably,  $B^*$  and  $B_N$  seem to coincide in a finite range, in agreement with theoretical predictions within the locally critical scenario [30,31]. Here, we suggest that magnetotransport measurements on pure  $\text{YbRh}_2\text{Si}_2$  under hydrostatic pressure will help to clarify this central point about the understanding of quantum criticality in this heavy fermion metal.

## References

- [1] *G. R. Stewart*, Rev. Mod. Phys. **73** (2001) 797; *ibid.* **78** (2006) 743.
- [2] See, e. g., *H. v. Löhneysen et al.*, Rev. Mod. Phys. **79** (2007) 1015, and references therein.
- [3] *S. Doniach*, Physica B **91** (1977) 231.
- [4] *J. Custers et al.*, Nature **424** (2003) 524.
- [5] *P. Gegenwart et al.*, Phys. Rev. Lett. **89** (2002) 056402.
- [6] *S. Paschen et al.*, Nature **432** (2004) 881.
- [7] *P. Gegenwart et al.*, Science **315** (2007) 969.
- [8] *P. Gegenwart et al.*, Physica B **403** (2008) 1184.
- [9] *S. Ernst, S. Kirchner, C. Krellner, C. Geibel, G. Zwirgmaier, F. Steglich, and S. Wirth*, Nature Vol **474** (2011) 362.
- [10] *S. Friedemann et al.*, Phys. Rev. B **82** (2010) 035103.
- [11] *O. Trovarelli et al.*, Phys. Rev. Lett. **85** (2000) 626 (2000).
- [12] *S. Danzenbächer et al.*, Phys. Rev. B **75** (2007) 045109.
- [13] *O. Stockert et al.* Physica B **378** (2006) 157.
- [14] *J. Kroha et al.*, Physica E **18** (2003) 69.
- [15] *M. Maltseva, M. Dzero, and P. Coleman*, Phys. Rev. Lett. **103** (2009) 206402.
- [16] *J. Figgins and D. K. Morr*, Phys. Rev. Lett. **104** (2010) 187202.
- [17] *T. A. Costi*, Phys. Rev. Lett. **85** (2000) 1504.
- [18] *U. Köhler, N. Oeschler, F. Steglich, S. Maquilon, and Z. Fisk*, Phys. Rev. B **77** (2008) 104412.
- [19] *B. Cornut and B. Coqblin*, Phys. Rev. B **5** (1972) 4541.
- [20] *P. Coleman, C. Pépin, Q. Si, and R. Ramazashvili*, J. Phys. Condens. Matter **13** (2001) R723.
- [21] *J. A. Hertz*, Phys. Rev. B **14** (1976) 1165.
- [22] *A. J. Millis*, Phys. Rev. B **48** (1993) 7183.
- [23] *T. Moriya and T. Takimoto*, J. Phys. Soc. Jpn. **64**, (1995) 960.
- [24] *S. Friedemann et al.*, Proc. Natl. Acad. Sci USA **107** (2010) 14547.
- [25] *S. Friedemann et al.*, J. Phys.: Condens. Matter **23** (2011) 094216.
- [26] *S. Friedemann et al.*, Nature Phys. **5** (2009) 422.
- [27] *S. Friedemann et al.*, in Scientific Report 2006-2008, p. 99 (Max Planck Institute for Chemical Physics of Solids, Dresden Germany, 2009).
- [28] *Y. Tokiwa, P. Gegenwart, C. Geibel, and F. Steglich*, J. Phys. Soc. Jpn. **78** (2009) 123708.
- [29] *P. Coleman*, Phys. Status Solidi B **247** (2010) 506.
- [30] *Q. Si*, Phys. Status Solidi B **378** (2006) 23.
- [31] *Q. Si*, Phys. Status Solidi B **247** (2010) 457.

<sup>1</sup> Present address: Cavendish Laboratory, JJ Thomson Avenue, Cambridge CB3 0HE, United Kingdom

<sup>2</sup> I. Physics Institute, Georg-August-Universität, 37077 Göttingen, Germany

<sup>3</sup> MPI for the Physics of Complex Systems Dresden, 01187 Dresden, Germany

<sup>4</sup> Institute of Solid State Physics, Vienna University of Technology, 1040 Vienna, Austria

<sup>5</sup> Department of Physics and Astronomy, Rice University, Houston, Texas 77005-1892, USA

<sup>6</sup> Institute for Mathematical Physics, Technical University Braunschweig, Germany